Inorg. Chem. **2004**, *43*, 6557−6567

Factors Affecting the Solid-State Structure and Dimensionality of Mercury Cyanide/Chloride Double Salts, and NMR Characterization of Coordination Geometries

Neil D. Draper,[†] Raymond J. Batchelor,[†] Pedro M. Aguiar,[‡] Scott Kroeker,*[,‡] and Daniel B. Leznoff*[,†]

Departments of Chemistry, Simon Fraser University, 8888 University Drive, Burnaby, British Columbia V5A 1S6, Canada, and University of Manitoba, Winnipeg, Manitoba R3T 2N2, Canada

Received February 16, 2004

In the reaction of organic monocationic chlorides or coordinatively saturated metal–ligand complex chlorides with linear, neutral $Hg(CN)_2$ building blocks, the Lewis-acidic $Hg(CN)_2$ moieties accept the chloride ligands to form mercury cyanide/chloride double salt anions that in several cases form infinite 1-D and 2-D arrays. Thus, $[PPN][Hg(CN)_2Cl]\cdot H_2O$ (**1**), $[^nBu_4N][Hg(CN)_2Cl]\cdot 0.5\ H_2O$ (**2**), and $[Ni(terpy)_2][Hg(CN)_2Cl]_2$ (**4**) contain $[Hg(CN)_2Cl]_2^{2-}$ anionic dimers ([PPN]Cl = bis(triphenylphosphoranylidene)ammonium chloride, $[^nBu_4N]Cl$ = tetrabutylammonium chloride, terpy = 2,2′:6′,6″-terpyridine). $[Cu(en)_2][Hg(CN)_2Cl]_2$ (**5**) is composed of alternating 1-D chloride-bridged $[Hg(CN)_2Cl]_n^{n-}$ ladders and cationic columns of $[Cu(en)_2]^{2+}$ (en = ethylenediamine). When $[Co(en)_3]Cl_3$ is reacted with 3 equiv of $Hg(CN)_2$, 1-D $\{[Hg(CN)_2]_2Cl\}_n^{n-}$ ribbons and $[Hg(CN)_2Cl_2]^{2-}$ moieties are formed; both form hydrogen bonds to $[Co(en)_3]^{3+}$ cations, yielding $[Co(en)_3][Hg(CN)_2Cl_2]\{[Hg(CN)_2]_2Cl\}$ (**6**). In $[Co(NH_3)_6]_2[Hg(CN)_2]_5Cl_6\cdot 2H_2O$ (**7**), $[Co(NH_3)_6]^{3+}$ cations and water molecules are sandwiched between chloride-bridged 2-D anionic $\{[Hg(CN)_2]_5Cl_6\}_n^{6n-}$ layers, which contain square cavities. The presence (or absence), number, and profile of hydrogen bond donor sites of the transition metal amine ligands were observed to strongly influence the structural motif and dimensionality adopted by the anionic double salt complex anions, while cation shape and cation charge had little effect. ^{199}Hg chemical shift tensors and $^1J(^{13}C,^{199}Hg)$ values measured in selected compounds reveal that the NMR properties are dominated by the $Hg(CN)_2$ moiety, with little influence from the chloride bonding characteristics. $\delta_{iso}(^{13}CN)$ values in the isolated dimers are remarkably sensitive to the local geometry.

Introduction

Research into the chemistry of supramolecular coordination polymers has rapidly grown in recent years due to an increased demand for functional materials with tunable properties.[1−7] The self-assembly of simple molecular building blocks containing organic ligands and inorganic metal ions provides an efficient and reliable approach for the design and synthesis of such organic/inorganic hybrid materials.[8−10] The characteristics of both the inorganic and organic moieties, such as available coordination sites, coordination geometry preference, ligand flexibility, and hydrogen bond interactions, ideally control the extended structure, thereby creating enormous potential for complexity and functionality of these modular materials.[11−18] Thus, with a careful selection

* Corresponding authors. E-mail: dleznoff@sfu.ca (D.B.L.); Scott_Kroeker@UManitoba.ca (S.K.). Phone: 1-604-291-4887 (D.B.L.); 1-204-474-9335 (S.K.). Fax: 1-604-291-3765 (D.B.L.); 1-204-474-7608 (S.K.).

† Simon Fraser University.

‡ University of Manitoba.

(1) Caulder, D. L.; Raymond, K. N. *Acc. Chem . Res.* **1999**, *32*, 975−982.
(2) Fujita, M. *Chem. Soc. Rev.* **1998**, *27*, 417−425.
(3) Jones, C. J. *Chem. Soc. Rev.* **1998**, *27*, 289−299.
(4) Janiak, C. *J. Chem. Soc., Dalton Trans.* **2003**, 2781−2804.
(5) Chen, C. T.; Suslick, K. S. *Coord. Chem. Rev.* **1993**, *128*, 293−322.
(6) Yaghi, O. M.; O'Keeffe, M.; Ockwig, N. W.; Chae, H. K.; Eddaoudi, M.; Kim, J. *Nature* **2003**, *423*, 705−714.
(7) Mitzi, D. B. *J. Chem. Soc., Dalton Trans.* **2001**, 1−12.
(8) Moulton, B.; Zaworotko, M. J. *Chem. Rev.* **2001**, *101*, 1629−1658.
(9) Eddaoudi, M.; Moler, D. B.; Li, H. L.; Chen, B. L.; Reineke, T. M.; O'Keeffe, M.; Yaghi, O. M. *Acc. Chem . Res.* **2001**, *34*, 319−330.
(10) Holliday, B. J.; Mirkin, C. A. *Angew. Chem., Int. Ed.* **2001**, *40*, 2022−2043.
(11) Ciurtin, D. M.; Smith, M. D.; zur Loye, H. C. *J. Chem. Soc., Dalton Trans.* **2003**, 1245−1250.
(12) Hoskins, B. F.; Robson, R. *J. Am. Chem. Soc.* **1990**, *112*, 1546−1554.
(13) Gardner, G. B.; Venkataraman, D.; Moore, J. S.; Lee, S. *Nature* **1995**, *374*, 792−795.
(14) Keller, S. W. *Angew. Chem., Int. Ed.* **1997**, *36*, 247−248.
(15) Xu, Z. M.; White, S.; Thompson, L. K.; Miller, D. O.; Ohba, M.; Ōkawa, H.; Wilson, C.; Howard, J. A. K. *J. Chem. Soc., Dalton Trans.* **2000**, *11*, 1751−1757.

10.1021/ic049792e CCC: $27.50
Published on Web 09/18/2004

of ligand, metal center(s), and reaction conditions, control over the architecture of the resultant structural motifs can be achieved.[11−17]

Systems that employ cyanometalate building blocks in concert with simple metal ions or their coordinatively unsaturated complexes to create multidimensional networks were among the first prepared coordination polymers to be studied and are of great current interest.[19−21] Alteration of the metal center in $[M(CN)_n]^{x-}$ building blocks and the consequent adjustment of the geometric, magnetic, and electronic properties provide the control and flexibility required to assemble solids with tunable properties.[19,21,22] This is illustrated by Prussian blue analogues such as the three-dimensional $\{Cr(II)_3\}[Cr(III)(CN)_6]_2 \cdot 10H_2O$[23] and $\{V(II)\}_\alpha\{V(III)_{(1-\alpha)}\}[Cr(III)(CN)_6]_{0.86} \cdot 2.8H_2O$ ($\alpha = 0.42$),[24,25] two molecule-based magnets that exhibit magnetic ordering at the high magnetic ordering temperatures of 240 and 315 K, respectively. Cyanometalates have also been employed extensively to generate inclusion compounds, clathrates, and zeolite-type systems that act as ion exchangers, molecular sieves, or materials for storing gases.[26−29] Typically, cyano-bridging square-planar or tetrahedral $[M(CN)_4]^{2-}$ (M = Ni, Pt, Pd, Cd) units are used to link various cationic transition metal−ligand complexes to prepare these multidimensional structures.[30,31]

Compared with octahedral, tetrahedral, and square-planar cyanometalates, linear metal cyanides have been relatively neglected. Although linear copper(I) cyanide has been used to form several versatile $\{Cu(CN)\}_n$ chain substructures, the resulting Cu(I) atoms typically have a trigonal planar geometry.[21,32,33] We are currently examining the use of mercury(II) cyanide, $Hg(CN)_2$, a virtually unexplored, linear, but neutral building block, to create supramolecular architectures. Our previous work has demonstrated that $Hg(CN)_2$ units can be incorporated into coordination polymers via bridging cyano groups that link to a coordinatively unsaturated transition metal center as found in $\{Cu(tmeda)[Hg(CN)_2]_2\}HgCl_4$, a noncentrosymmetric two-dimensional layer system that shows strong optical anisotropy (tmeda = *N*,*N*,*N*′,*N*′-tetramethylethylenediamine).[34] The $Hg(CN)_2$ unit is also known to react with simple salts such as MX (M = Na, K, Rb, Cs; X = NCO, NCS, N_3, CN, Cl, Br, I; sometimes HgX_2 is also added) to yield solid-state "double salt" arrays of the form $M^{n+}Hg(CN)_2X_n$ ($n = 1, 2$).[35,36] In these reactions, the Lewis-acidity of the Hg(II) center is the key feature controlling the reactivity. Thus, the coordinatively unsaturated Hg(II) center can accept compatible ligands during polymer formation to form square-planar, tetrahedral, or higher coordinate moieties in situ, in some cases increasing the structural and magnetic dimensionality of the system as a result.[37,38] At the same time, the cyano-N atoms of the $Hg(CN)_2$ unit, if not bound to another metal, can participate in hydrogen bonding. These may be either simple or bifurcated hydrogen bonds of the CN···H−X type (where X is an electronegative atom) and can play an important role in the packing and stabilization of the structures formed.[39] Recently, molecular recognition of anionic cyanometalates as hydrogen bond acceptor sites to bis-amidinium dicationic tectons has been employed in the rational design of 1-D and 2-D hydrogen bonded molecular networks.[40] N-cyano hydrogen bonding has also been proposed as a possible exchange path for magnetic interactions.[41,42]

We have prepared several coordination polymers containing mercury cyanide/chloride double salt building blocks, such as $[Hg(CN)_2Cl]^-$, that aggregate in different structural motifs that include one-dimensional ladders and ribbons, and two-dimensional layers, depending on the accompanying cation. Herein, we investigate the possible factors influencing the structure of the anionic motif formed, including cation shape, cation charge, and hydrogen bonding interactions. Selected compounds are characterized by ^{199}Hg and ^{13}C MAS NMR to explore the dependence of the NMR properties on mercury coordination geometry.

(16) Orr, G. W.; Barbour, L. J.; Atwood, J. L. *Science* **1999**, *285*, 1049−1052.
(17) Yaghi, O. M.; Li, H. L.; Davis, C.; Richardson, D.; Groy, T. L. *Acc. Chem. Res.* **1998**, *31*, 474−484.
(18) Chesnut, D. J.; Hagrman, D.; Zapf, P. J.; Hammond, R. P.; LaDuca, R.; Haushalter, R. C.; Zubieta, J. *Coord. Chem. Rev.* **1999**, *192*, 737−769.
(19) Černák, J.; Orendáč, M.; Potočňák, I.; Chomič, J.; Orendáčová, A.; Skoršepa, J.; Feher, A. *Coord. Chem. Rev.* **2002**, *224*, 51−66.
(20) Sharpe, A. G. *The Chemistry of Cyano Complexes of the Transition Metals*; Academic Press: London, 1976.
(21) Dunbar, K. R.; Heintz, R. A. *Prog. Inorg. Chem.* **1997**, *45*, 283−391.
(22) Kahn, O.; Larionova, J.; Ouahab, L. *Chem. Commun.* **1999**, 945−952.
(23) Mallah, T.; Thiébaut, S.; Verdaguer, M.; Veillet, P. *Science* **1993**, *262*, 1554−1557.
(24) Ferlay, S.; Mallah, T.; Ouahes, R.; Veillet, P.; Verdaguer, M. *Nature* **1995**, *378*, 701−703.
(25) Verdaguer, M.; Bleuzen, A.; Marvaud, V.; Vaissermann, J.; Seuleiman, M.; Desplanches, C.; Scuiller, A.; Train, C.; Garde, R.; Gelly, G.; Lomenech, C.; Rosenman, I.; Veillet, P.; Cartier, C.; Villain, F. *Coord. Chem. Rev.* **1999**, *192*, 1023−1047.
(26) Kaemper, M.; Wagner, M.; Weiss, A. *Angew. Chem., Int. Ed.* **1979**, *91*, 517−518.
(27) Kondo, M.; Okubo, T.; Asami, A.; Noro, S.; Yoshitomi, T.; Kitagawa, S.; Ishii, T.; Matsuzaka, H.; Seki, K. *Angew. Chem., Int. Ed.* **1999**, *38*, 140−143.
(28) Kondo, M.; Shimamura, M.; Noro, S.; Minakoshi, S.; Asami, A.; Seki, K.; Kitagawa, S. *Chem. Mater.* **2000**, *12*, 1288−1299.
(29) Seki, K.; Mori, W. *J. Phys. Chem. B* **2002**, *106*, 1380−1385.
(30) Iwamoto, T. In *Comprehensive Supramolecular Chemistry*; Atwood, J. L., Lehn, J. M., Eds.; Pergamon: New York, 1996; Vol. 7, pp 643−690.
(31) Iwamoto, T. In *Inclusion Compounds*; Atwood, J. L., Davies, J. E. D., MacNicol, D. D., Eds.; Academic Press: London, 1984; Vol. 5, pp 177−208.
(32) Chesnut, D. J.; Zubieta, J. *Chem. Commun.* **1998**, 1707−1708.
(33) Chesnut, D. J.; Kusnetzow, A.; Birge, R.; Zubieta, J. *J. Chem. Soc., Dalton Trans.* **2001**, 2581−2586.
(34) Draper, N. D.; Batchelor, R. J.; Sih, B. C.; Ye, Z. G.; Leznoff, D. B. *Chem. Mater.* **2003**, *15*, 1612−1616.
(35) Thiele, G.; Hilfrich, P. *Z. Anorg. Allg. Chem.* **1980**, *461*, 109−124.
(36) Thiele, G.; Brodersen, K.; Frohring, H. *Z. Naturforsch., B: Chem. Sci.* **1981**, *36B*, 180−187.
(37) Leznoff, D. B.; Draper, N. D.; Batchelor, R. J. *Polyhedron* **2003**, *22*, 1735−1743.
(38) Draper, N. D.; Batchelor, R. J.; Leznoff, D. B. *Cryst. Growth Des.* **2004**, *4*, 621−632.
(39) Li, D. F.; Gao, S.; Zheng, L. M.; Sun, W. Y.; Okamura, T.; Ueyama, N.; Tang, W. X. *New J. Chem.* **2002**, *26*, 485−489.
(40) Ferlay, S.; Bulach, V.; Félix, O.; Hosseini, M. W.; Planeix, J. M.; Kyritsakas, N. *CrystEngComm.* **2002**, 447−453.
(41) Orendáč, M.; Orendáčová, A.; Černák, J.; Feher, A. *Solid State Commun.* **1995**, *94*, 833−835.
(42) Černák, J.; Chomič, J.; Gravereau, P.; Orendáčová, A.; Orendáč, M.; Kovač, J.; Feher, A.; Kappenstein, C. *Inorg. Chim. Acta* **1998**, *281*, 134−140.

Experimental Section

CAUTION: Mercury(II) salts are very toxic and should be handled with care.

General Procedures and Physical Measurements. All manipulations were performed in air using purified solvents. All reagents were obtained from commercial sources and used as received. IR spectra were obtained using a Thermo Nicolet 670 FT-IR spectrometer. Microanalyses (C, H, N) were performed at Simon Fraser University by Mr. Miki Yang.

Solid-State NMR. ^{199}Hg MAS NMR spectra were obtained at 107.4 MHz (B_0 = 14.1 T) on a Varian Inova 600 spectrometer. Powder samples (~120 mg) were packed into 5 mm rotors and spun at 6−8 kHz. Spectra were collected using direct polarization with an rf field of 50 kHz and short pulse lengths corresponding to a 12−15° tip angle, to ensure homogeneous excitation across the full spectral region. About 20k transients were acquired, with a relaxation delay of 4 s. Chemical shifts are cited relative to dimethylmercury, measured by the secondary standard, sodium tetraethylammonium tetracyanomercurate, which is a single peak at −434 ppm with respect to $Hg(CH_3)_2$.[43] Chemical shift tensor principal components were obtained by simulating the experimental spectrum using the STARS software (Varian, Inc.).

^{13}C CPMAS NMR spectra were collected at 125.8 MHz (B_0 = 11.7 T) and 150.8 MHz (B_0 = 14.1 T) on Bruker AMX500 and Varian Inova 600 spectrometers, respectively. Magic-angle spinning at 6−8 kHz was done with 5 mm double-resonance probes. Standard cross-polarization from ^{1}H was optimized for observation of cyanide signals, resulting in contact times of about 4−7 ms; about 2000 transients were acquired with relaxation delays of 25 s. Chemical shifts are referenced to TMS, using the secondary standard adamantane, possessing peaks at 38.6 and 29.5 ppm.

Synthetic Procedures. [PPN][Hg(CN)$_2$Cl]·H$_2$O (1). To a 10 mL MeOH/H_2O (50/50% vol) solution of bis(triphenylphosphoranylidene)ammonium chloride ([PPN]Cl; 0.136 g, 0.24 mmol) was added a 10 mL aqueous solution of $Hg(CN)_2$ (0.059 g, 0.23 mmol) with stirring. The solution was concentrated by slow evaporation. Colorless platelets of [PPN][Hg(CN)$_2$Cl]·H_2O (**1**) were collected by vacuum filtration, washed with cold methanol, and left to air-dry. Yield: 0.163 g (84%). Anal. Calcd for $C_{38}H_{32}N_3ClHgOP_2$: C, 54.03; H, 3.82; N, 4.97. Found: C, 54.01; H, 3.87; N, 4.84. IR (KBr, cm^{-1}): 3056 (m), 3034 (w), 2819 (w), 2694 (w), 2215 (w), 2173 (w, ν_{CN}), 2051 (w), 1918 (w), 1829 (m), 1711 (m), 1588 (m), 1482 (m), 1438 (s), 1363(w), 1283 (s), 1265 (vs), 1182 (m), 1115 (vs), 1028 (m), 998 (m), 857 (w), 799 (m), 745 (m), 722 (vs), 693 (vs), 550 (vs), 534 (vs), 496 (s).

[^{n}Bu$_4$N][Hg(CN)$_2$Cl]·0.5 H$_2$O (2). To a 10 mL aqueous solution of tetrabutylammonium chloride ([^{n}Bu$_4$N]Cl; 0.055 g, 0.20 mmol) was added a 10 mL aqueous solution of $Hg(CN)_2$ (0.050 g, 0.20 mmol) with stirring. The solution was concentrated by slow evaporation. Colorless blocks of [^{n}Bu$_4$N][Hg(CN)$_2$Cl]·0.5H_2O (**2**) were collected by vacuum filtration, washed with cold methanol, and left to air-dry. Yield: 0.108 g (59%). Anal. Calcd for $C_{18}H_{37}N_3ClHgO_{0.5}$: C, 40.07; H, 6.91; N, 7.79. Found: C, 39.85; H, 6.87; N, 7.83. IR (KBr, cm^{-1}): 3599 (s), 3506 (s), 2963 (vs), 2935 (vs), 2876 (vs), 2734 (w), 2408 (w), 2180 (w, ν_{CN}), 2175 (w, ν_{CN}), 2150 (w, ν_{CN}), 1836 (w), 1844 (w), 1829 (w), 1793 (w), 1750 (m), 1711 (s), 1652 (m), 1635 (m), 1484 (s), 1463 (s), 1419 (m), 1383 (s), 1364 (s), 1223 (s), 1178 (w), 1152 (m), 1108 (m), 1091 (w), 1056 (m), 1026 (m), 883 (s), 799 (m), 739 (s), 530 (m), 417 (s), 407 (s).

[(C$_6$H$_5$)$_4$As][Hg(CN)$_2$Cl] (3). To a 10 mL aqueous solution of tetraphenylarsonium chloride ([$(C_6H_5)_4$As]Cl; 0.083 g, 0.20 mmol) was added a 10 mL aqueous solution of $Hg(CN)_2$ (0.050 g, 0.20 mmol) with stirring. The solution was concentrated by slow evaporation. Colorless blocks of [$(C_6H_5)_4$As][Hg(CN)$_2$Cl] (**3**) were collected by vacuum filtration, washed with cold methanol, and left to air-dry. Yield: 0.091 g (68%). Anal. Calcd for $C_{26}H_{20}N_2AsClHg$: C, 46.51; H, 3.00; N, 4.17. Found: C, 46.46; H, 3.03; N, 4.14. IR (KBr, cm^{-1}): 3520 (m), 3452 (m), 3156 (w), 3080 (w), 3058 (m), 3021 (w), 2991 (w), 2657 (w), 2563 (w), 2172 (w, ν_{CN}), 2162 (w, ν_{CN}), 1980 (w), 1904 (w), 1826 (w), 1776 (w), 1676 (w), 1632 (w), 1578 (w), 1483 (m), 1439 (s), 1420 (m), 1339 (m), 1308 (m), 1184 (m), 1161 (w), 1081 (s), 1022 (w), 997 (s), 925 (w), 853 (w), 742 (s), 689 (s), 613 (w), 479 (s), 466 (s).

[Ni(terpy)$_2$][Hg(CN)$_2$Cl]$_2$ (4). To a 5 mL aqueous solution of $NiCl_2$·$6H_2O$ (0.015 g, 0.063 mmol) was added a 5 mL methanolic solution of 2,2′:6′,6″-terpyridine (terpy; 0.030 g, 0.128 mmol). While stirring, a 5 mL aqueous solution of $Hg(CN)_2$ (0.032 g, 0.127 mmol) was added to this solution. The mixture was concentrated by slow evaporation. Brown crystal bars of [Ni(terpy)$_2$][Hg(CN)$_2$Cl]$_2$ (**4**) were collected by vacuum filtration, washed with cold H_2O followed by cold methanol, and left to air-dry. Yield: 0.050 g (72%). Anal. Calcd. for $C_{34}H_{22}N_{10}Cl_2Hg_2Ni$: C, 37.08; H, 2.01; N, 12.72. Found: C, 37.34; H, 1.97; N, 12.62. IR (KBr, cm^{-1}): 3732 (w), 3108 (m), 3074 (m), 3030 (m), 2172 (w, ν_{CN}), 2012 (w), 1978 (w), 1879 (w), 1600 (s), 1574 (m), 1563 (m), 1475 (s), 1470 (s), 1450 (s), 1419 (m), 1405 (w), 1321 (m), 1297 (w), 1248 (m), 1184 (m), 1160 (m), 1094 (w), 1052 (w), 1032 (m), 1016 (s), 904 (w), 830 (w), 774 (s), 740 (w), 667 (w), 650 (m), 513 (w), 436 (w), 412 (m).

[Cu(en)$_2$][Hg(CN)$_2$Cl]$_2$ (5). To a 10 mL aqueous solution of $CuCl_2$·$2H_2O$ (0.068 g, 0.40 mmol) was added an aqueous solution of ethylenediamine (en; stock solution, 0.80 mmol). While stirring, a 10 mL aqueous solution of $Hg(CN)_2$ (0.202 g, 0.80 mmol) was added to this solution. The mixture was concentrated by slow evaporation. Purple crystal bars of [Cu(en)$_2$][Hg(CN)$_2$Cl]$_2$ (**5**) were collected by vacuum filtration, washed with cold H_2O followed by cold methanol, and left to air-dry. Yield: 0.285 g (94%). Anal. Calcd for $C_8H_{16}N_8Cl_2CuHg_2$: C, 12.64; H, 2.12; N, 14.75. Found: C, 12.52; H, 2.14; N, 14.63. IR (KBr, cm^{-1}): 3338 (s), 3324 (s), 3294 (s), 3276 (s), 3262 (s), 3233 (s), 3143 (m), 2993 (w), 2968 (m), 2955 (m), 2897 (m), 2175 (m, ν_{CN}), 1709 (m), 1617 (m), 1591 (s), 1458 (m), 1362 (w), 1323 (w), 1274 (m), 1232 (w), 1179 (m), 1095 (m), 1039 (s), 1010 (m), 974 (m), 881 (w), 719 (m), 695 (m), 536 (m), 423 (m), 413 (m).

[Co(en)$_3$][Hg(CN)$_2$Cl$_2$]{[Hg(CN)$_2$]$_2$Cl} (6). To a 10 mL aqueous solution of $[Co(en)_3]Cl_3$ (0.076 g, 0.22 mmol) was added a 20 mL aqueous solution of $Hg(CN)_2$ (0.151 g, 0.60 mmol). The mixture was concentrated by slow evaporation. Orange crystal platelets of [Co(en)$_3$][Hg(CN)$_2$Cl$_2$]{[Hg(CN)$_2$]$_2$Cl} (**6**) were collected by vacuum filtration, washed with cold H_2O followed by cold methanol, and left to air-dry. Yield: 0.137 g (62%). Anal. Calcd for $C_{12}H_{24}N_{12}Cl_3CoHg_3$: C, 13.06; H, 2.19; N, 15.23. Found: C, 12.84; H, 2.10; N, 14.93. IR (KBr, cm^{-1}): 3266 (vs), 3233 (vs), 3162 (vs), 3133 (vs), 2904 (w), 2750 (w), 2612 (w), 2189 (w, ν_{CN}), 2185 (w, ν_{CN}), 1620 (m), 1583 (m), 1566 (m), 1508 (w), 1462 (m), 1398 (w), 1366 (w), 1320 (m), 1298 (m), 1240 (w), 1149 (m), 1053 (s), 1003 (m), 881 (w), 785 (m), 582 (m), 552 (w), 495 (w), 438 (s).

[Co(NH$_3$)$_6$]$_2$[Hg(CN)$_2$]$_5$Cl$_6$·2H$_2$O (7). To a 10 mL aqueous solution of $[Co(NH_3)_6]Cl_3$ (0.064 g, 0.24 mmol) was added a 20 mL aqueous solution of $Hg(CN)_2$ (0.150 g, 0.59 mmol). The mixture was concentrated by slow evaporation. Large orange crystal platelets of $[Co(NH_3)_6]_2[Hg(CN)_2]_5Cl_6$·$2H_2O$ (**7**) were collected by vacuum

(43) Eichele, K.; Kroeker, S.; Wu, G.; Wasylishen, R. E. *Solid State NMR* **1995**, *4*, 295−300.

Table 1. Summary of Crystallographic Data for **1**, **2**, and **4**−**7**[a]

	1	**2**	**4**	**5**	**6**	**7**
empirical formula	$C_{38}H_{32}N_3ClHgOP_2$	$C_{18}H_{37}N_3ClHgO_{0.5}$	$C_{34}H_{22}N_{10}Cl_2Hg_2Ni$	$C_8H_{16}N_8Cl_2CuHg_2$	$C_{12}H_{24}N_{12}Cl_3CoHg_3$	$C_{10}H_{40}N_{22}Cl_6Co_2Hg_5O_2$
fw (g mol^{-1})	844.67	539.55	1101.39	759.90	1103.46	1834.10
T (K)	293	293	293	293	293	293
cryst syst	monoclinic	monoclinic	triclinic	triclinic	triclinic	monoclinic
space group	$P2_1/n$	$P2_1/n$	$P\bar{1}$	$P\bar{1}$	$P\bar{1}$	$I2/m$
a (Å)	10.949(2)	12.580(2)	8.840(2)	6.3063(13)	8.393(1)	8.5648(9)
b (Å)	12.761(3)	14.710(4)	12.509(3)	8.132(3)	11.853(3)	12.8938(13)
c (Å)	25.921(6)	13.075(2)	17.779(4)	9.9615(18)	13.838(3)	19.0120(15)
α (deg)	90	90	92.488(19)	70.43(2)	100.12(2)	90
β (deg)	90.414(17)	94.189(14)	91.35(2)	85.675(18)	91.51(2)	97.088(6)
γ (deg)	90	90	110.442(19)	72.63(2)	105.94(2)	90
Z	4	4	2	1	2	2
U (Å^3)	3621.6	2413.1	1838.9	459.2	1299.1	2083.5
D_{calc} (g cm^{-3})	1.549	1.485	1.989	2.748	2.821	2.924
2θ limits (deg)	4−45	4−45	4−45	4−54	4−50	4−51
reflns collected	5104	3384	5073	2091	4614	2055
indep reflns	4753	3175	4850	2018	4583	2049
reflns obsd [$I \geq 2.5\sigma(I)$]	2505	1475	2722	1689	3086	1347
GOF on F	1.250	1.548	1.269	1.835	1.661	1.212
R_1, R_w [$I \geq 2.5\sigma(I)$][b]	0.038, 0.043	0.034, 0.036	0.034, 0.035	0.027, 0.030	0.040, 0.046	0.032, 0.043

[a] Enraf-Nonius CAD-4 diffractometer, Mo Kα radiation ($\lambda = 0.71069$ Å), graphite monochromator. [b] Function minimized $\sum w(|F_o| - |F_c|)^2$ where $w^{-1} = \sigma^2(F_o) + 0.0002F_o^2$, $R_1 = \sum||F_o| - |F_c||/\sum|F_o|$, $R_w = (\sum w(|F_o| - |F_c|)^2/\sum w|F_o|^2)^{1/2}$.

filtration, washed with cold H_2O followed by cold methanol, and left to air-dry. Yield: 0.196 g (92%). Anal. Calcd for $C_{10}H_{40}N_{22}Cl_6Co_2Hg_5O_2$: C, 6.56; H, 2.20; N, 16.80. Found: C, 6.42; H, 2.20; N, 16.55. IR (KBr, cm^{-1}): 3625 (s), 3448 (m), 3258 (vs), 2771 (m), 2667 (m), 2632 (w), 2180 (s, ν_{CN}), 1869 (w), 1844 (w), 1771 (m), 1612 (vs), 1412 (m), 1357 (s), 1324 (s), 844 (s), 428 (s).

X-ray Crystallographic Analysis of 1, 2, and 4−**7.** Crystallographic data for structures **1**, **2**, and **4**−**7** are collected in Table 1. All crystals were mounted on glass fibers using epoxy adhesive. Crystal descriptions for each compound are as follows: **1** was a colorless block having dimensions 0.11 × 0.14 × 0.20 mm^3; **2** was a colorless block having dimensions 0.12 × 0.18 × 0.23 mm^3; **4** was a brown platelet having dimensions 0.03 × 0.11 × 0.34 mm^3; **5** was a purple platelet having dimensions 0.05 × 0.15 × 0.34 mm^3; **6** was an orange platelet having dimensions 0.03 × 0.17 × 0.23 mm^3; **7** was an orange platelet having dimensions 0.05 × 0.23 × 0.31 mm^3. The data were collected at room temperature using the diffractometer control program DIFRAC[44] and an Enraf Nonius CAD4F diffractometer employing graphite monochromated Mo Kα radiation. The following data ranges were recorded: **1** = 4° ≤ 2θ ≤ 45°; **2** = 4° ≤ 2θ ≤ 45°; **4** = 4° ≤ 2θ ≤ 45°; **5** = 4° ≤ 2θ ≤ 54°; **6** = 4° ≤ 2θ ≤ 50°; **7** = 4° ≤ 2θ ≤ 51°. The data were corrected by integration for the effects of absorption using a semiempirical ψ-scan method with the following transmission ranges: **1** = 0.4566−0.5756; **2** = 0.2694−0.3599; **4** = 0.2039−0.4446; **5** = 0.0482−0.2188; **6** = 0.0424−0.2103; **7** = 0.0106−0.0460. Data reduction for all compounds included corrections for Lorentz and polarization effects. Final unit-cell dimensions were determined on the basis of the following well-centered reflections: **1** = 26 reflections with range 29° ≤ 2θ ≤ 30°; **2** = 28 reflections with range 30° ≤ 2θ ≤ 32°; **4** = 24 reflections with range 30° ≤ 2θ ≤ 34°; **5** = 19 reflections with range 40° ≤ 2θ ≤ 49°; **6** = 26 reflections with range 40° ≤ 2θ ≤ 45°; **7** = 40 reflections with range 34° ≤ 2θ ≤ 35°.

For compounds **5**, **6**, and **7**, coordinates and anisotropic displacement parameters for the non-hydrogen atoms were refined; for compounds **1**, **2**, and **4** all non-cyano carbon and oxygen atoms were refined using isotropic thermal parameters. Hydrogen atoms were placed in calculated positions (d C−H 0.95 Å; d N−H 0.93 Å, d O−H 0.85 Å), and their coordinate shifts were linked with those of the respective carbon, nitrogen, or oxygen atoms during refinement. Isotropic thermal parameters for the hydrogen atoms were initially assigned proportionately to the equivalent isotropic thermal parameters of their respective carbon, nitrogen, or oxygen atoms. Subsequently, the isotropic thermal parameters for the C−H hydrogen atoms were constrained to have identical shifts during refinement, as were those of the N−H and O−H hydrogen atoms. Extinction parameters[45] were included in the final cycles of full-matrix least-squares refinement of **2**, **6**, and **7**. Selected bond lengths and angles for **1**, **2**, and **4** are found in Table 2, while those of **5**, **6**, and **7** are found in Tables 3, 4, and 5, respectively.

Table 2. Selected Bond Lengths (Å) and Angles (deg) for the $[Hg(CN)_2Cl]_2^{2-}$ Dimers of **1**[a], **2**[b], and **4**[c]

selected atoms	**1**	**2**	**4**
	Bond Lengths		
Hg(1)−Cl(1)	2.713(3)	2.747(3)	2.751(3), 2.711(4)
Hg(1)−Cl(1*)	2.766(3)	2.766(3)	2.799(4), 2.820(3)
Hg(1)−C(11)	2.054(15)	2.056(16)	2.052(15), 2.044(17)
Hg(1)−C(12)	2.054(15)	2.02(2)	2.060(17), 2.060(16)
C(11)−N(11)	1.121(14)	1.107(14)	1.121(16), 1.143(16)
C(12)−N(12)	1.104(15)	1.126(19)	1.114(17), 1.130(16)
	Bond Angles		
Cl(1)−Hg(1)−Cl(1*)	85.48(9)	93.10(9)	82.44(10), 87.73(10)
Hg(1)−Cl(1)−Hg(1*)	94.52(9)	86.90(9)	97.56(10), 92.27(10)
C(11)−Hg(1)−C(12)	150.7(5)	160.1(6)	150.5(6), 158.1(6)
Hg(1)−C(11)−N(11)	175.9(13)	177.5(14)	177.4(14), 175.2(17)
Hg(1)−C(11)−N(12)	175.9(14)	175 (2)	177.9(17), 179.8(14)

[a] Symmetry transformations: (*) $-x + 2$, $-y + 1$, $-z + 2$. [b] Symmetry transformations: (*) $-x + 1$, $-y + 1$, $-z + 2$. [c] Symmetry transformations: (*) $-x + 1$, $-y + 1$, $-z + 1$. The second values pertain to the second dimer of compound **4**. Symmetry transformations: (*) $-x$, $-y + 3$, $-z + 2$.

The programs used for all absorption corrections, data reduction, and processing of **1**, **2**, and **4**−**7** were from the *NRCVAX* Crystal Structure System.[46] The structures were refined using *CRYSTALS*.[47] Complex scattering factors for neutral atoms[48] were used in the calculation of structure factors.

(44) Gabe, E. J.; White, P. S.; Enright, G. D. *DIFRAC: A Fortran 77 Control routine for 4-Circle Diffractometers*; N.R.C.: Ottawa, 1995.
(45) Larsen, A. C. In *Crystallographic Computing*; Ahmed, F. R., Ed.; Munksgaard: Copenhagen, 1970; p 291.
(46) Gabe, E. J.; Lepage, Y.; Charland, J. P.; Lee, F. L.; White, P. S. *J. Appl. Crystallogr.* **1989**, *22*, 384−387.

Results

Synthesis and Characterization of 1−7. The reaction of an aqueous/methanolic solution of bis(triphenylphosphoranylidene)ammonium chloride ([PPN]Cl), tetrabutylammonium chloride ([^{n}Bu$_4$N]Cl), or tetraphenylarsonium chloride ([(C$_6$H$_5$)$_4$As]Cl) with an aqueous solution containing 1 equiv of Hg(CN)$_2$ yielded single crystals of [PPN][Hg(CN)$_2$Cl]·H$_2$O (**1**), [^{n}Bu$_4$N][Hg(CN)$_2$Cl]·0.5H$_2$O (**2**), and [(C$_6$H$_5$)$_4$As][Hg(CN)$_2$Cl] (**3**), respectively. Similarly, the reaction of an aqueous solution of NiCl$_2$ with 2 equiv of 2,2′:6′,2″-terpyridine (terpy), or an aqueous solution of CuCl$_2$ with 2 equiv of ethylenediamine (en), with 2 equiv of Hg(CN)$_2$ yielded single crystals of [Ni(terpy)$_2$][Hg(CN)$_2$Cl]$_2$ (**4**) and [Cu(en)$_2$][Hg(CN)$_2$Cl]$_2$ (**5**). Complete migration of the labile chloride ligands from the harder Ni(II) and Cu(II) centers to the coordinatively unsaturated, softer Hg(II) center drives the formation of **4** and **5**.[49,50] Similarly, reaction of an aqueous solution of [Co(en)$_3$]Cl$_3$ with 3 equiv of Hg(CN)$_2$ or [Co(NH$_3$)$_6$]Cl$_3$, with 2.5 equiv of Hg(CN)$_2$, yielded **6** and **7**, respectively, but their resulting double salt formulas were more complex, as described below. For every product, this halide migration to the Lewis-acidic Hg(CN)$_2$ moiety generates nonlinear Hg(II) complex anions with coordination numbers greater than two, sometimes increasing the structural dimensionality in the process. The IR spectra of **1**−**7** clearly show the presence of the cyano groups. The ν_{CN} bands range from 2162 cm^{-1} (**3**) to 2185 cm^{-1} (**5**) and are consistent with terminal cyanide groups on nonlinear Hg(II) units with coordination numbers greater than two such as that found for K[Hg(CN)$_2$Cl] (ν_{CN} = 2170 cm^{-1}).[36] These bands are shifted from the 2194 cm^{-1} absorbance of Hg(CN)$_2$.[51] The solid-state structures of complexes **1**−**7** are described below.

Structures of the [Hg(CN)$_2$Cl]$^-$ Anion with [PPN]$^+$, [^{n}Bu$_4$N]$^+$, and [Ni(terpy)$_2$]$^{2+}$ Cations. All three structures consist of isolated [Hg(CN)$_2$Cl]$_2^{2-}$ anionic dimers and two [PPN]$^+$ (**1**) (Figure 1), two [^{n}Bu$_4$N]$^+$ (**2**), and one [Ni(terpy)$_2$]$^{2+}$ (**4**) cations, respectively; the [(C$_6$H$_5$)$_4$As]$^+$ (**3**) cation also appears to be balanced by the same [Hg(CN)$_2$Cl]$_2^{2-}$ unit as shown by a low resolution crystal structure. The bond lengths and angles for the [Hg(CN)$_2$Cl]$_2^{2-}$ anions in **1**, **2**, and **4** are gathered in Table 2.

IR spectroscopy studies have shown that in solution the coordinatively unsaturated Hg(II) center of mercury cyanide can accept a chloride ligand to form the anionic [Hg(CN)$_2$Cl]$^-$ moiety.[52,53] For compounds **1**−**4**, these [Hg(CN)$_2$Cl]$^-$ units exist as [Hg(CN)$_2$Cl]$_2^{2-}$ dimers in the solid-state with

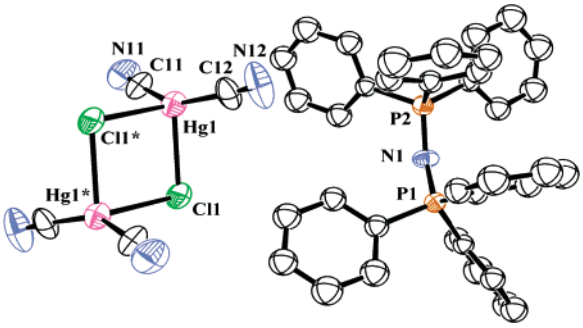

Figure 1. Structure of [PPN][Hg(CN)$_2$Cl]·H$_2$O (**1**). The second [PPN]$^+$ cation, disordered H$_2$O molecule, and hydrogen atoms have been omitted for clarity (ORTEP, 50% ellipsoids).

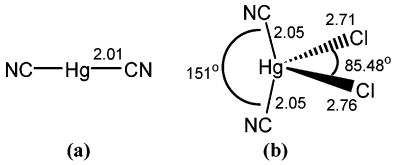

Figure 2. Examples of (a) linear characteristic coordination (x = 2) in Hg(CN)$_2$ and (b) effective seesaw coordination based on linear characteristic coordination (2 + 2) of a Hg(II) center in **1**.

C−Hg−C angles ranging from 150.5(6)° (**4**) to 160.1(6)° (**2**), and Cl−Hg−Cl angles ranging from 82.44(10)° (**4**) to 93.10(9)° (**2**). According to the convention devised by Grdenić,[54] ligands coordinated to Hg(II) centers can be classified into two types. Where all x bond lengths are equivalent in an HgL$_x$ system, the mercury atom has a characteristic coordination number x and an associated geometry; for Hg(II), characteristic coordination numbers of two, with a linear geometry, are particularly prevalent (Figure 2a).[54,55] The effective coordination number and geometry includes all ligands within the van der Waals radii sums and is represented as (x + y); only when x = 2, 3 can additional ligands be accommodated.[54] Thus, two (or more) groups of bond lengths are cited to define the effective coordination (x + y): the shortest group (x) represents the characteristic coordination number and geometry of the mercury center, while the longer groups (y) represent weaker interactions of ligands with the metal as determined by X-ray crystallographic structures.[54,56] Taken together, these different bond length groups often result in highly distorted geometries (Figure 2b).

Each Hg(II) center in compounds **1**−**4** has a seesaw effective coordination geometry based upon linear characteristic coordination (2 + 2 according to Grdenić).[54] The Hg(1)−Cl bond lengths range from 2.711(4) to 2.820(3) Å, which can be compared with the 2.589(5) and 2.614(5) Å found for [^{n}Bu$_4$N][HgCl$_3$][57] and the 2.562(3) and 2.827(3) Å found for the related [Hg$_2$Cl$_6$]$^{2-}$ anionic dimers in

(47) Watkin, D. J.; Prout, C. K.; Carruthers, J. R.; Betteridge, P. W.; Cooper, R. I. *CRYSTALS* Issue 12.16; Chemical Crystallography Laboratory, University of Oxford: Oxford, England, 2001.
(48) International Union of Crystallography. *International tables for X-ray crystallography*; Kynoch Press: Birmingham, England, 1952.
(49) Wang, S. N.; Trepanier, S. J.; Zheng, J. C.; Pang, Z.; Wagner, M. J. *Inorg. Chem.* **1992**, *31*, 2118−2127.
(50) Exarchos, G.; Robinson, S. D.; Steed, J. W. *Polyhedron* **2001**, *20*, 2951−2963.
(51) Ashurst, K. G.; Finkelstein, N. P.; Goold, L. A. *J. Chem. Soc. A* **1971**, 1899−1902.
(52) Penneman, R. A.; Jones, L. H. *J. Inorg. Nucl. Chem.* **1961**, *20*, 19−31.
(53) Brodersen, K.; Hummel, H.-U. In *Comprehensive Coordination Chemistry*, 1st ed.; Wilkinson, G., Gillard, R. D., McCleverty, J. A., Eds.; Pergamon Press: Oxford, 1987; Vol. 5; pp 1048−1088.
(54) Grdenić, D. *Q. Rev.* **1965**, *19*, 303−328.
(55) Cotton, F. A.; Wilkinson, G.; Murillo, C. A.; Bochmann, M. *Advanced Inorganic Chemistry*, 6th ed.; Wiley: New York, 1999.
(56) House, D. A.; Robinson, W. T.; McKee, V. *Coord. Chem. Rev.* **1994**, *135*, 533−586.
(57) Goggin, P. L.; King, P.; McEwan, D. M.; Taylor, G. E.; Woodward, P.; Sandstroem, M. *J. Chem. Soc., Dalton Trans.* **1982**, 875−882.

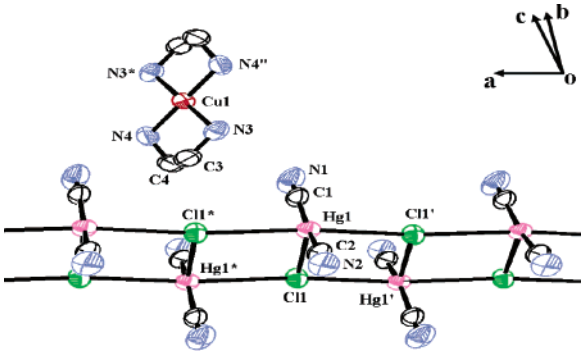

Figure 3. Structure of $[Cu(en)_2][Hg(CN)_2Cl]_2$ (**5**) showing an extended 1-D $[Hg(CN)_2Cl]_n^{n-}$ anionic ladder (ORTEP, 50% ellipsoids). Only one $[Cu(en)_2]^{2+}$ cation is shown, and hydrogen atoms have been omitted for clarity.

Table 3. Selected Bond Lengths (Å) and Angles (deg) for $[Cu(en)_2][Hg(CN)_2]_2Cl]_2$ (**5**)[a]

selected atoms	bond length	selected atoms	bond length
Hg(1)−C(1)	2.066(8)	N(1)−C(1)	1.103(10)
Hg(1)−C(2)	2.072(7)	N(2)−C(2)	1.064(9)
Hg(1)−Cl(1)	2.709(2)	N(3)−C(3)	1.475(10)
Hg(1)−Cl(1*)	3.0972(15)	N(4)−C(4)	1.476(12)
Hg(1)−Cl(1′)	3.2195(16)	Cu(1)−N(3)	1.986(6)
C(3)−C(4)	1.487(13)	Cu(1)−N(4)	2.011(6)
selected atoms	**bond angle**	**selected atoms**	**bond angle**
C(1)−Hg(1)−C(2)	162.9(3)	Cl(1)−Hg(1)−Cl(1*)	85.90(6)
Hg(1)−C(1)−N(1)	178.6(8)	Cl(1)−Hg(1)−Cl(1′)	88.04(5)
Hg(1)−C(2)−N(2)	176.4(7)	Cl(1*)−Hg(1)−Cl(1′)	173.41(7)
Cl(1)−Hg(1)−C(1)	97.1(3)	Hg(1)−Cl(1)−Hg(1*)	94.10(6)
Cl(1)−Hg(1)−C(2)	99.8(2)	Hg(1)−Cl(1)−Hg(1′)	91.96(5)
Cl(1*)−Hg(1)−C(1)	92.31(19)	Hg(1*)−Cl(1)−Hg(1′)	173.41(7)
Cl(1′)−Hg(1)−C(1)	91.10(19)	N(3)−Cu(1)−N(4)	84.8(3)
Cl(1*)−Hg(1)−C(2)	91.51(19)	N(3)−Cu(1)−N(4″)	95.2(3)
Cl(1′)−Hg(1)−C(2)	86.96(19)		

[a] Symmetry transformations: (*) $-x+1, -y, -z-1$; (′) $-x+2, -y, -z-1$; (″) $-x+2, -y+1, -z$.

$[Cu(en)_2][Hg_2Cl_6]$.[58] No hydrogen bonds are present between the cations and $[Hg(CN)_2Cl]_2^{2-}$ dimers of compounds **1**−**4** since $[PPN]^+$, $[^nBu_4N]^+$, $[(C_6H_5)_4As]^+$, and $[Ni(terpy)_2]^{2+}$ lack any significant hydrogen donor sites; no increase in structural dimensionality is observed for compounds **1**−**4**. The disordered water molecules in **1** and the half equivalent of water in **2** do not have an impact on the structure or dimensionality of the $[Hg(CN)_2Cl]_2^{2-}$ anionic dimer as no water is present in **3** or **4**.

Structure of $[Cu(en)_2][Hg(CN)_2Cl]_2$ (5). The X-ray crystal structure of $[Cu(en)_2][Hg(CN)_2Cl]_2$ (**5**) reveals dimeric units of $[Hg(CN)_2Cl]_2^{2-}$ that are linked via weak Hg(1)−Cl(1′) interactions resulting in a 1-D $[Hg(CN)_2Cl]_n^{n-}$ anionic ladder motif that runs parallel to the *a*-axis (Figure 3). The bond lengths and angles for **5** are gathered in Table 3. The ladder frame and rungs are made up of three very different Hg−Cl bonds (2.709(2), 3.0972(15), and 3.2195(16) Å), leaving the cyano ligands lying in the *bc*-plane. These bond lengths are well within the sum of the Hg/Cl van der Waals radii of 3.30 Å[54,59] and are comparable to the bridging Hg−Cl bond lengths (3.051(2) and 3.217(2) Å) found in $\{Cu(tmeda)[Hg(CN)_2]_2\}[HgCl_4]$.[34]

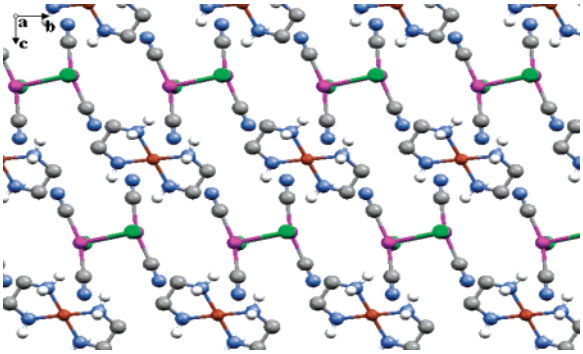

Figure 4. Complex **5**, viewed down the *a*-axis, showing alternating rows of $[Cu(en)_2]^{2+}$ columns and $[Hg(CN)_2Cl]_n^{n-}$ ladders. Ethyl hydrogen atoms have been omitted for clarity. Color scheme: Hg, pink; Cu, red; Cl, green; N, blue; C, gray; H, white.

The Hg(II) centers have an effective square pyramidal coordination geometry based upon linear characteristic coordination (2 + 1 + 1 + 1). Two chloride and two cyano ligands occupy the basal plane while the third (but closest) chloride ligand occupies the apical site. The Cu(II) center in **5** has a distorted square planar geometry composed of two ethylenediamine ligands. An N-cyano ligand can be found in proximity to each open Cu(II) axial site with a Cu(1)···NC distance of 2.772(7) Å.

Two types of hydrogen bonds are formed between $[Cu(en)_2]^{2+}$ cations and the $[Hg(CN)_2Cl]_n^{n-}$ anionic ladders, consisting of N−H···Cl and N−H···NC donor/acceptor pairs, that result in a three-dimensional, bimetallic network (Figure 4). The $[Cu(en)_2]^{2+}$ cations form weak hydrogen bonds (range: N(3)−N(1) = 3.182 Å to N(4)−N(2) = 3.389 Å) to different $[Hg(CN)_2Cl]_n^{n-}$ anionic ladders, resulting in a 3-D network of alternating rows of $[Cu(en)_2]^{2+}$ cationic columns and $[Hg(CN)_2Cl]_n^{n-}$ ladders down the *a*-axis, where each cationic column is surrounded by four anionic ladders and vice versa. The particular inorganic/organic hybrid framework of **5** is very similar to those reported for [4,4′-H_2bipy][MCl_4] (M = Mn, Pb; bipy = 4,4′-bipyridine),[60,61] and (H_2DAH)BiI_5 (DAH = 1,6-hexanediamine).[62] Although what appear to be small channels that run parallel to the *a*-axis between each $[Hg(CN)_2Cl]_n^{n-}$ ladder in a row and the $[Cu(en)_2]^{2+}$ columns above and below are observed in **5**, a space-filling model (not shown) clearly shows the channels to be filled.

Structure of $[Co(en)_3][Hg(CN)_2Cl_2]\{[Hg(CN)_2]_2Cl\}$ (6). This complex contains a 1-D anionic ribbon composed of $\{[Hg(CN)_2]_2Cl\}^-$ units linked together via bridging Cl(1) atoms (Figure 5). The crystallographic inequivalence of the $\{[Hg(CN)_2]_2Cl\}^-$ units results in two sets of similar Hg−Cl bond lengths as presented in Table 4. Both Hg(1) and Hg(2) centers have effective seesaw geometries based upon linear characteristic coordination (2 + 1 + 1), while the quadruply bridging Cl(1) atom has a distorted square-planar geometry

(58) Schunk, A.; Thewalt, U. *Z. Anorg. Allg. Chem.* **2001**, *627*, 797−802.
(59) Bondi, A. *J. Phys. Chem.* **1964**, *68*, 441−451.
(60) Gillon, A. L.; Orpen, A. G.; Starbuck, J.; Wang, X. M.; Rodríguez-Martín, Y.; Ruiz-Pérez, C. *Chem. Commun.* **1999**, 2287−2288.
(61) Gillon, A. L.; Lewis, G. R.; Orpen, A. G.; Rotter, S.; Starbuck, J.; Wang, X. M.; Rodríguez-Martín, Y.; Ruiz-Pérez, C. *J. Chem. Soc., Dalton Trans.* **2000**, 3897−3905.
(62) Mitzi, D. B.; Brock, P. *Inorg. Chem.* **2001**, *40*, 2096−2104.

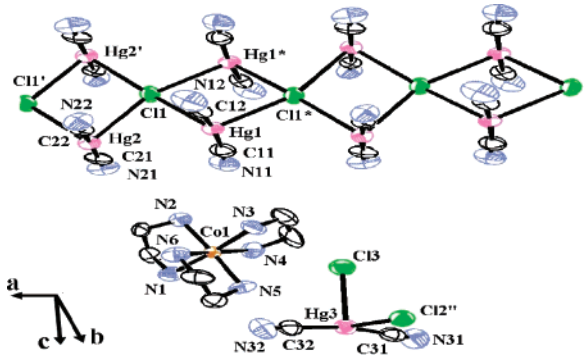

Figure 5. Structure of $[Co(en)_3][Hg(CN)_2Cl_2]\{[Hg(CN)_2]_2Cl\}$ (**6**) showing an extended 1-D $\{[Hg(CN)_2]Cl\}_n^{n-}$ anionic ribbon (ORTEP, 50% ellipsoids). Only one $[Co(en)_3]^{3+}$ cation and one $[Hg(CN)_2Cl_2]^{2-}$ anion have been shown. Hydrogen atoms have been omitted for clarity.

Table 4. Selected Bond Lengths (Å) and Angles (deg) for $[Co(en)_3][Hg(CN)_2Cl_2]\{[Hg(CN)_2]_2Cl\}$ (**6**)[a]

selected atoms	bond length	selected atoms	bond length
Hg(1)−C(11)	2.045(19)	Hg(2)−C(21)	2.019(15)
Hg(1)−C(12)	2.079(19)	Hg(2)−C(22)	2.053(15)
Hg(1)−Cl(1)	2.915(4)	Hg(3)−Cl(2″)	2.939(4)
Hg(1)−Cl(1*)	2.968(4)	Hg(3)−Cl(3)	2.823(4)
Hg(2)−Cl(1′)	2.950(4)	Hg(3)−C(31)	2.05(2)
Hg(2)−Cl(1)	3.112(4)	Hg(3)−C(32)	2.09(2)
Co(1)−N(1)	1.952(12)	Co(1)−N(4)	1.984(13)
Co(1)−N(2)	2.000(12)	Co(1)−N(5)	1.983(12)
Co(1)−N(3)	1.957(12)	Co(1)−N(6)	1.981(13)

selected atoms	bond angle	selected atoms	bond angle
Cl(1)−Hg(1)−C1(1*)	102.17(10)	Cl(2″)−Hg(3)−Cl(3)	93.48(11)
Cl(1)−Hg(1)−C(11)	91.8(5)	Cl(2″)−Hg(3)−C(31)	104.9(4)
Cl(1*)−Hg(1)−C(11)	94.5(5)	Cl(3)−Hg(3)−C(31)	92.8(4)
Cl(1)−Hg(1)−C(12)	92.7(5)	Cl(2″)−Hg(3)−C(32)	82.5(4)
Cl(1*)−Hg(1)−C(12)	91.3(4)	Cl(3)−Hg(3)−C(32)	97.3(4)
C(11)−Hg(1)−C(12)	171.7(6)	C(31)−Hg(3)−C(32)	167.1(6)
Cl(1′)−Hg(2)−C(21)	92.2(5)	Hg(1)−Cl(1)−Hg(1*)	77.83(11)
Cl(1′)−Hg(2)−C(22)	93.1(4)	Hg(1)−Cl(1)−Hg(2′)	170.6(2)
Cl(1)−Hg(2)−Cl(1′)	79.43(12)	Hg(1*)−Cl(1)−Hg(2′)	101.00(12)
Cl(1)−Hg(2)−C(21)	91.7(4)	Hg(1)−Cl(1)−Hg(2)	80.49(10)
Cl(1)−Hg(2)−C(22)	91.7(4)	Hg(1*)−Cl(1)−Hg(2)	158.29(15)
C(21)−Hg(2)−C(22)	174.1(5)	Hg(2)−Cl(1)−Hg(2′)	100.57(12)

[a] Symmetry transformations: (*) $-x, -y-1, -z+1$; (′) $-x+1, -y-1, -z+1$; (″) $-x, -y, -z+2$.

with two angles less than 90° and two angles greater than 90°.

In addition to the $\{[Hg(CN)_2]Cl\}_n^{n-}$ ribbon, an individual $[Hg(CN)_2Cl_2]^{2-}$ anionic moiety is present in **6**; this Hg(3) center also has an effective seesaw coordinate geometry based upon linear characteristic coordination (2 + 1 + 1). The $[Hg(CN)_2Cl_2]^{2-}$ unit does not show any significant interactions with the $\{[Hg(CN)_2]_2Cl\}_n^{n-}$ ribbon but forms a complex network of N−H···Cl and N−H···NC interactions between four different $[Co(en)_3]^{3+}$ cations (range: N(5)−N(31) = 3.197 Å to N(1)−Cl(3) = 3.744 Å). Each $[Co(en)_3]^{3+}$ cation also forms hydrogen bonds to different $\{[Hg(CN)_2]_2Cl\}_n^{n-}$ ribbons via N−H···NC interactions (range: N(22)−N(1) = 2.954 Å to N(12)−N(4) = 3.292 Å), thus resulting in the complex 3-D, bimetallic network shown in Figure 6. Rows of the $\{[Hg(CN)_2]_2Cl\}_n^{n-}$ ribbons are separated by columns consisting of the $[Co(en)_3]^{3+}$ and $[Hg(CN)_2Cl_2]^{2-}$ units along the *b*-axis. The resultant alternating anionic−cationic framework in **6** is very similar to that found in **5**.

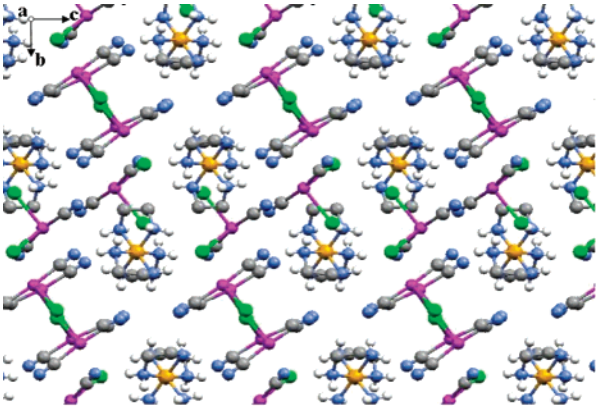

Figure 6. Interactions of ions in **6** as viewed down the *a*-axis. Ethyl hydrogen atoms have been omitted for clarity. Color scheme: Hg, pink; Co, orange; Cl, green; N, blue; C, gray; H, white.

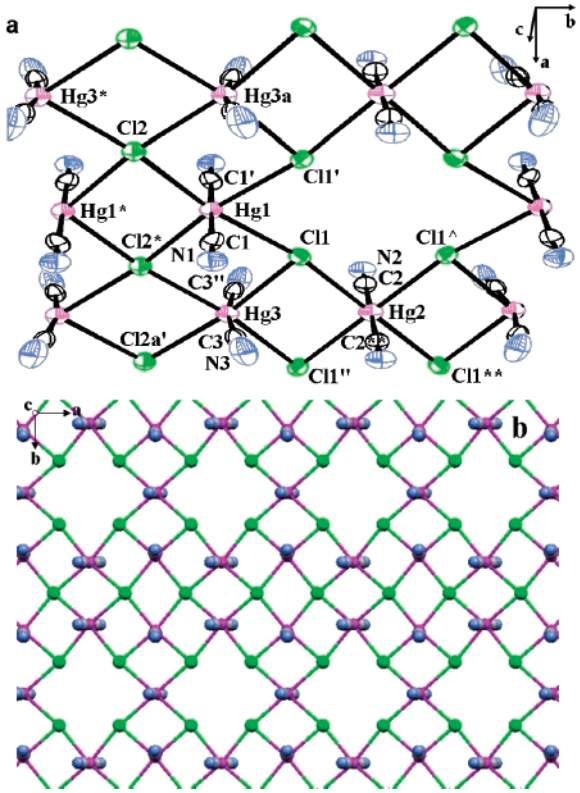

Figure 7. (a) Extended 2-D anionic layer structure of $[Co(NH_3)_6]_2[Hg(CN)_2]_5Cl_6{\cdot}2H_2O$ (**7**) (ORTEP, 50% ellipsoids); (b) arrangement of square cavities as viewed down the *c*-axis. $[Co(NH_3)_6]^{3+}$ cations and H_2O molecules have been omitted for clarity. Color scheme: Hg, pink; Cl, green; N, blue; C, gray.

Structure of $[Co(NH_3)_6]_2[Hg(CN)_2]_5Cl_6{\cdot}2H_2O$ (7). The X-ray single crystal structure of $[Co(NH_3)_6]_2[Hg(CN)_2]_5Cl_6{\cdot}2H_2O$ (**7**) reveals a 2-D anionic layer structure (Figure 7). This layer is composed of $Hg(CN)_2$ molecules and Cl^- ions, held together via Hg−Cl bridges (Table 5). Each Hg(II) center has a commonly observed[54] distorted octahedral effective geometry based upon linear characteristic coordination (2 + 4), composed of four chlorine groups parallel to, and two *trans*-cyano groups perpendicular to, the *ab*-plane. Each Cl(2) atom is quadruply bridging to different Hg(II) centers while each Cl(1) atom is only triply bridging to different Hg(II) centers (Figure 7a). Along the *b*-axis, double columns consisting of alternating Hg(1) and Hg(3) octahedra

Table 5. Selected Bond Lengths (Å) and Angles (deg) for $[Co(NH_3)_6]_2[[Hg(CN)_2]_5Cl_6]\cdot 2H_2O$ (**7**)[a]

selected atoms	bond length	selected atoms	bond length
Hg(1)−C(1)	2.025(11)	Hg(2)−Cl(1)	3.087(3)
Hg(2)−C(2)	2.032(12)	Hg(2)−Cl(1^)	3.087(3)
Hg(3)−C(3)	2.040(13)	Hg(1)−Cl(1)	3.119(3)
N(1)−C(1)	1.135(14)	Hg(1)−Cl(2)	3.078(3)
N(2)−C(2)	1.11(2)	Hg(3)−Cl(1)	3.072(2)
N(3)−C(3)	1.124(14)	Hg(3)−Cl(2*)	3.083(2)

selected atoms	bond angle	selected atoms	bond angle
C(1)−Hg(1)−C(1′)	180.0(6)	Cl(1)−Hg(2)−Cl(1″)	82.72(9)
C(2)−Hg(2)−C(2**)	180	Cl(1^)−Hg(2)−Cl(1″)	180
C(3)−Hg(3)−C(3″)	168.4(6)	Cl(1)−Hg(3)−Cl(2a′)	170.06(7)
Cl(1)−Hg(1)−Cl(1′)	78.35(9)	Cl(1)−Hg(3)−Cl(2*)	91.88(7)
Cl(1)−Hg(1)−Cl(2)	169.39(7)	Cl(1′)−Hg(3)−Cl(1″)	97.90(10)
Cl(1′)−Hg(1)−Cl(2)	91.10(6)	Cl(2*)−Hg(3)−Cl(2a′)	78.39(11)
Cl(1)−Hg(1)−Cl(2′)	91.10(6)	Hg(1)−Cl(1)−Hg(2)	169.86(9)
Cl(1′)−Hg(1)−Cl(2′)	169.39(7)	Hg(1)−Cl(1)−Hg(3)	88.01(6)
Cl(2)−Hg(1)−Cl(2′)	99.46(10)	Hg(2)−Cl(1)−Hg(3)	82.41(6)
Cl(1)−Hg(1)−C(1)	88.8(3)	Hg(1)−Cl(2)−Hg(1*)	80.54(10)
Cl(1′)−Hg(1)−C(1)	91.7(3)	Hg(1)−Cl(2)−Hg(3a)	88.544(19)
Cl(2)−Hg(1)−C(1)	89.2(3)	Hg(1)−Cl(2)−Hg(3*)	167.53(13)
Cl(2*)−Hg(1)−C(1)	90.9(3)	Hg(1)−Cl(2)−Hg(3)	167.53(13)
Cl(1)−Hg(2)−Cl(1**)	180	Hg(3*)−Cl(2)−Hg(3a)	101.61(11)
Cl(1)−Hg(2)−Cl(1^)	82.72(9)	Hg(3)−Cl(2)−Hg(3*b)	101.7(1)
Cl(1**)−Hg(2)−Cl(1^)	97.28(9)	Hg(3)−Cl(2)−Hg(3*b)	101.7(1)

[a] Symmetry transformations: (*) $-x+2, -y-1, -z$; (**) $-x+3, -y, -z$; (′) $-x+2, y, -z$; (″) $-x+3, y, -z$; (a) $x-1, y, z$; (a′) $x+1, y, z$; (^) $x, -y, z$.

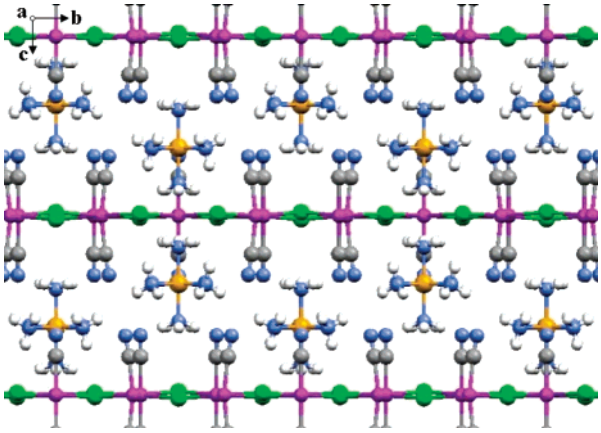

Figure 8. View of **7** down the *a*-axis, showing three $\{[Hg(CN)_2]_5Cl_6\}_n^{6n-}$ 2-D anionic nets with $[Co(NH_3)_6]^{3+}$ cations that lie above and below the cavities; H_2O molecules have been omitted for clarity. Color scheme: Hg, pink; Co, orange; Cl, green; N, blue; C, gray; H, white.

assemble, each sharing three Cl-edges. The Hg(2) centers link these double columns together along the *a*-axis by sharing the fourth Cl-edge of each Hg(3) octahedron. Since the fourth Cl-edge of each Hg(1) is left unshared, a series of square cavities arranged in columns along the *b*-axis (Figure 7b) is formed in the $\{[Hg(CN)_2]_5Cl_6\}_n^{6n-}$ layer as defined by four Hg(1)−Cl(1)−Hg(2) edges.

The $[Co(NH_3)_6]^{3+}$ cations and H_2O molecules are located above and below the cavities (Figure 8). Several hydrogen bonds are formed from the NH_3 ligands to the chloride and the cyano ligands atoms of neighboring nets (range: N(3)−N(7) = 3.065 Å to N(4)−Cl(1) = 3.703 Å). The water molecules also form a series of hydrogen bonds to the $[Co(NH_3)_6]^{3+}$ cations (O(1)−N(7) = 3.085 Å, O(1)−N(5) 3.130 Å), and to the anionic layers (O(1)−N(2) = 3.091 Å, O(1)−N(3) = 3.483 Å). The result is a 3-D network of

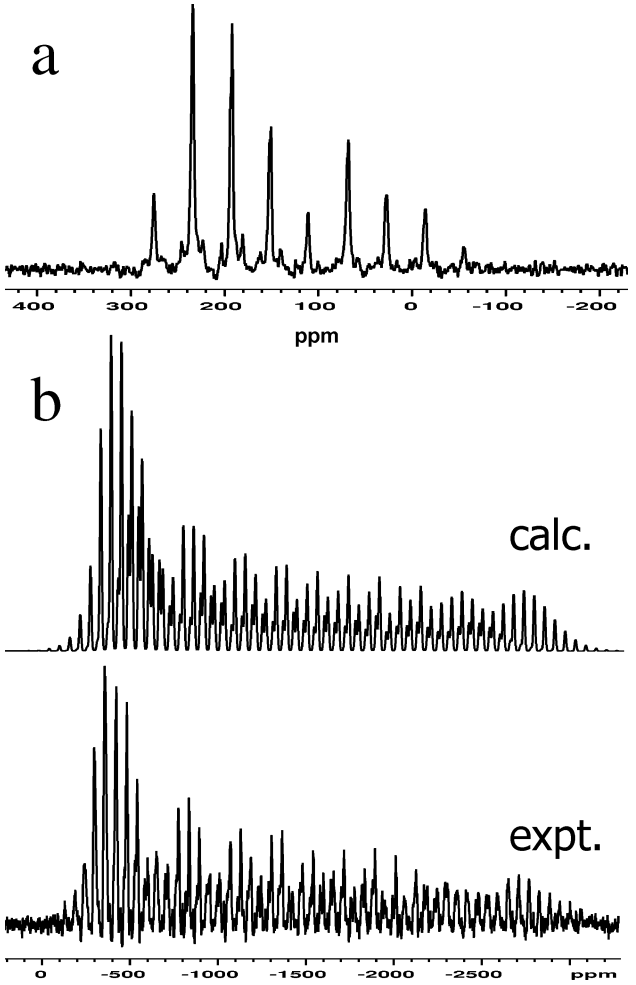

Figure 9. NMR spectra of **7** at 14.1 T: (a) ^{13}C CPMAS; (b) ^{199}Hg MAS, with comparison to two-site simulation based on parameters in Table 6.

$[Co(NH_3)_6]^{3+}$ cations and water molecules sandwiched between 2-D $\{[Hg(CN)_2]_5Cl_6\}_n^{6n-}$ anionic layers. The nets are shifted relative to each other such that the cavities from different nets do not stack into channel generating columns.

The $\{[Hg(CN)_2]_5Cl_6\}_n^{6n-}$ anionic layer of **7** is similar to the corrugated $[Hg(CN)_2I]^-$ anionic layers observed in $K[Hg(CN)_2I]$,[63] which consist of iodide-edge-sharing HgI_4-$(CN)_2$ octahedra along the equatorial plane forming the anionic layers with the K^+ cations intercalating the layers; however, unlike **7**, cavities are not present in these anionic layers. $[NH_3(C_2H_5)]_2[Hg(CN)_2Cl_2]$, a 2-D layer perovskite-like material, contains square cavities arranged in a chessboard manner, similar to **7**, with the $[NH_3(C_2H_5)]^+$ cations located both above and below each cavity.[64]

Solid-State NMR Studies. The diamagnetic compounds **1**, **2**, **6**, and **7** were examined by ^{199}Hg and ^{13}C MAS NMR.

^{199}Hg NMR. Despite repeated attempts using cross-polarization and direct polarization, with long acquisition times and extensive parameter optimization, no ^{199}Hg signals could be observed for **1** and **2**. This may be due to motional dynamics of the isolated $[Hg(CN)_2Cl]_2$ dimers, which are

(63) Kruse, F. H. *Acta Crystallogr.* **1963**, *16*, 105−109.
(64) Zouari, R.; Bensalah, A.; Daoud, A.; Rothammel, W.; Burzlaff, H. *Acta Crystallogr., Sect. C* **1993**, *49*, 1596−1598.

Table 6. NMR Data for Mercury Cyanide/Chloride Double Salts[a]

		^{199}Hg						^{13}C	
	sites	δ_{11}	δ_{22}	δ_{33}	δ_{iso}	Ω	κ	δ_{iso}	$^1J(^{13}C,^{199}Hg)$
1	Hg,CN(11) Hg,CN(12)							144.4 ± 0.5	
2	Hg,CN(1) Hg,CN(2)							166.5 ± 0.5 169.0 ± 0.5	
6	Hg(1),CN(11) Hg(1),CN(12) Hg(2),CN(21) Hg(2),CN(22) Hg(3),CN(31) Hg(3),CN(32)	98	98	−3301	−1035 ± 90	3400 ± 300	+1	148.5 ± 0.5 150.6 ± 0.5	3250 ± 50 3250 ± 50
7	Hg(1),CN(1) Hg(2),CN(2) Hg(3),CN(3)	−295 −416	−295 −416	−2995 −2696	−1195 ± 2 −1176 ± 2	2700 ± 100 2300 ± 100	+1 +1	150 ± 0.5, 151 ± 0.5	3420 ± 40, 3420 ± 40

[a] Chemical shifts in ppm, and *J* couplings in Hz.

less connected to the framework than the related units in **6** and **7**, for which ^{199}Hg signals were observed.

Compound **6** contains one-dimensional anionic chains comprising two crystallographically distinct Hg centers, and a third Hg unit not in the chain (Figure 5). The ^{199}Hg MAS NMR spectrum (not shown) is not of sufficient quality to identify all three sites; however, the overall envelope of spinning sideband peaks indicates nearly axially symmetric chemical shielding anisotropy spanning about 3400 ± 300 ppm. The isotropic chemical shift of the observed site is estimated to be −1035 ± 90 ppm (i.e., one of three possible isotropic peaks).

The ^{199}Hg MAS NMR spectrum of **7** is shown in Figure 9 along with the calculated spectrum based on a two-site model (Table 6). One signal is assigned to both Hg(1) and Hg(2), because of their very similar geometry (e.g., C−Hg−C ≈ 180°), and the second site represents Hg(3), with its distinct local environment (e.g., C−Hg−C ≈ 169°); the spectrum does not support a three-site model.

This approach results in an approximately 2:1 intensity ratio, with the lower intensity site (Hg(3)) about 19 ± 2 ppm higher in frequency (i.e., less shielded) than that of Hg(1) and Hg(2). The Hg(3) shielding anisotropy is also somewhat smaller than that of Hg(1) and Hg(2) (Ω = 2300 vs 2700 ppm), with all three components of the shielding tensor shifting to yield the net reduction in span (Table 6). Both observations are consistent with known ^{199}Hg shielding trends with geometry (see Discussion section).

^{13}C NMR. ^{13}C CPMAS spectra of **1** and **2** reflect significant differences in the cyanide local environment, despite apparently similar $[Hg(CN)_2Cl]_2$ dimeric units. Compound **1** shows a single resonance at 144.4 ppm, whereas **2** has two cyanide peaks at 169.0 and 166.5 ppm.

Compound **6** exhibits a cyanide signal with maxima at 148.5 and 150.6 ppm. The breadth and shape of the peak indicate that this is a composite signal representing all six crystallographically inequivalent cyanides with slightly different geometries. The relative intensities suggest that four of the cyanide groups make up the lower frequency peak, and two are at the higher frequency; however, there is no obvious structural basis for assignments. In addition to a large central peak representing ^{13}C nuclei bonded to spin-inactive isotopes of mercury (^{198}Hg, ^{200}Hg, ^{202}Hg, ^{204}Hg; natural abundance totalling 69.8%), two pairs of satellite peaks are observed from *J*-coupling to the spin-$^1/_2$ ^{199}Hg (natural abundance 16.9%), both of which correspond to $^1J(^{13}C,^{199}Hg)$ of 3250 ± 50 Hz. In principle, there should also be a weaker quartet from *J*-coupling to spin-$^3/_2$ ^{201}Hg (natural abundance 13.2%); however, the quadrupolar nature of this isotope often broadens these peaks to obscurity (see Discussion section).

Compound **7** consists of a composite peak with maxima at 150 and 151 ppm, presumably representing all three CN species in the compound (Figure 9a). These are not clearly differentiated at either magnetic field, and the geometries do not permit convenient assignment. Satellite peaks indicate $^1J(^{13}C,^{199}Hg)$ = 3420 ± 40 Hz for the set of cyanide signals.

All ^{13}C MAS NMR spectra contain coupling to the cyano ^{14}N. Due to the quadrupolar nature of ^{14}N (spin-1, 99.6% natural abundance), the dipolar coupling to ^{13}C is not completely averaged by magic-angle spinning. The residual dipolar coupling and the small *J*-coupling of about 5−10 Hz[65] manifest as an asymmetric "doublet" at these magnetic fields.[66] In the present case, the ^{13}C line widths (ca. 2 ppm) are too large to resolve these features (typical parameters predict a peak separation of 1.1 ppm at 11.7 T and 0.75 ppm at 14.1 T); however, in some cases they appear as asymmetry in the peakshape. While this effect can be eliminated by the use of isotopic enrichment in spin-$^1/_2$ ^{15}N,[67−69] the potential benefits were deemed insufficient to justify the expense and synthetic effort of labeling.

^{13}C CPMAS spectra exhibited spinning sidebands spanning 300−350 ppm. Due to complications arising from overlapping cyanide peaks, coupling to ^{14}N and ^{199}Hg, and generally low sensitivity for slow-spinning ^{13}C CPMAS spectra of

(65) Wasylishen, R. E.; Lenkinski, R. E.; Rodger, C. *Can. J. Chem.* **1982**, *60*, 2113-2117.
(66) Hexem, J. G.; Frey, M. H.; Opella, S. J. *J. Am. Chem. Soc.* **1981**, *103*, 224−226.
(67) Curtis, R. D.; Ratcliffe, C. I.; Ripmeester, J. A. *J. Chem. Soc., Chem. Commun.* **1992**, 1800−1802.
(68) Kroeker, S.; Wasylishen, R. E.; Hanna, J. V. *J. Am. Chem. Soc.* **1999**, *121*, 1582−1590.
(69) Kroeker, S.; Wasylishen, R. E. *Can. J. Chem.* **1999**, *77*, 1962−1972.

natural abundance cyanide, no attempts to quantify anisotropic shielding tensors were made. However, the observed spinning sidebands suggest that the chemical shift tensors are qualitatively similar to other typical cyanide ligands reported in the literature, namely, nearly axially symmetric with the unique component most shielded ($\kappa \sim +1$) and $\Omega \approx 300-350$ ppm.[69−71]

Discussion

In an effort to account for the wide range of structural motifs found for $[Hg(CN)_2Cl]^-$ double salt and related anions, structures **1**−**7** can be examined by considering the effects of (a) cation shape, (b) cation charge, and (c) hydrogen bonding interactions from the amine transition metal-bound ligands. All of the transition metal cations utilized in this study were coordinatively saturated by the amine ligands, thus eliminating any potential for either chloride or N-cyano coordination to the transition metal center.

Influence of Cation Shape. By examining structures **1**−**3**, the effect that cation shape has on the $[Hg(CN)_2Cl]^-$ anionic motif can be determined. All three compounds are salts of 1:1 stoichiometry, with organic monocations, and most importantly, the cations all lack significant hydrogen bonding donor or acceptor sites. Although interactions between the $[PPN]^+$ phenyl groups, or terpyridine rings, with the anions of the type C−H···X, C−H···NC, and Hg···π,[72,73] contribute to the net stabilization of the crystal lattice formed, they are quite weak and do not appear to strongly influence the final anionic structure. As described above, all three structures form $[Hg(CN)_2Cl]_2^{2-}$ anionic dimers regardless of whether the cation has a dumbbell ($[PPN]^+$, **1**), a tetrahedral ($[^nBu_4N]^+$, **2**), or a propeller ($[(C_6H_5)_4As]^+$, **3**) shape. Thus, the difference in cation shape has no apparent effect on the anionic motif; no significant templating is occurring.

Influence of Cation Charge. In order to investigate the effect of cation charge, structure **4** with its $[Ni(terpy)_2]^{2+}$ cation is compared with the +1 cations of structures **1**−**3**. The use of 2 equiv of terpy constrains the Ni(II) center to be coordinatively saturated while it simultaneously eliminates possible strong hydrogen bond donor/acceptor pairs between the cation and anion. Despite the increased cation charge, no structural change is observed for the anionic motif of structure **4**; only $[Hg(CN)_2Cl]_2^{2-}$ dimers are formed. Efforts to yield single crystals from the reaction of $[Fe(terpy)_2]Cl_3$ and $Hg(CN)_2$ in order to investigate the effect of a cation with a +3 charge were unsuccessful.

Influence of Hydrogen Bonding Interactions. Comparison of the crystal structures of **5**−**7** allows the effects of hydrogen bond interactions of the cations on the $[Hg(CN)_2Cl]_n^{n-}$ double salt structural diversity to be investigated. The presence, number, and profile of hydrogen bond donor sites of the transition metal amine ligands strongly influence the structural motif adopted by the anionic double salt complex. When no N−H hydrogen bond donor sites are present, as in **1**−**4**, $[Hg(CN)_2Cl]_2^{2-}$ dimers are formed. The four $N-H_2$ donors of the two en ligands in **5** direct the formation of a 1-D $[Hg(CN)_2Cl]_n^{n-}$ anionic ladder, while the six $N-H_2$ donors of structure **6** direct the formation of a 1-D $\{Hg(CN)_2]_2Cl\}_n^{n-}$ anionic ribbon with additional $[Hg(CN)_2Cl_2]^{2-}$ units also present. It should be noted that the complex cations $[Cu(en)_2]^{2+}$ and $[Co(en)_3]^{3+}$ have different charges; the effect of cation charge does not seem to influence the anion structure, as discussed above. In **7**, the six $N-H_3$ donors of the $[Co(NH_3)_6]^{3+}$ cations and the water molecules direct the formation of 2-D anionic layers of $\{[Hg(CN)_2]_5Cl_6\}_n^{6n-}$. Thus, in general, an increase in the number of hydrogen bonding donor sites on the transition metal complex cation appears to increase the structural dimensionality of the anionic double salt from zero (**1**−**4**) to one- and two-dimensional (**5**−**7**). Organic cations with strong hydrogen bonding capability ought to induce similar structural direction of the double salt anions, as was observed with the $[4,4'\text{-}H_2bipy]^{2+}$ dications used in the formation of several perhalometalate solid-state structures.[60,61] It is not merely the number of hydrogen bond donors that controls the formation of the polymeric complex anions, but also the flexibility of the d^{10} Hg(II) center to adopt different effective coordination geometries (seesaw, square pyramidal, octahedral) that plays an important role in the type of anionic motif formed. The concept of direction anionic halometalate networks with organic moieties has recently been employed to fabricate new zeolite-type materials $(HNMe_3)[CuZn_5Cl_{12}]$ and $(H_2NEt_2)[CuZn_5Cl_{12}]$,[74] modular polymeric chlorocadmate(II) compounds,[75−77] and other structure types patterned after known chalcogenides.[78]

NMR Parameters and Structure. The available ^{199}Hg NMR parameters can be placed in the context of previous ^{199}Hg NMR studies of inorganic solids.[79−82] Compound **6**, involving four-coordinate mercury centers, has roughly similar chemical shielding to **7**, which has six-coordinate mercury. Despite this difference in coordination environment, both mercury types possess nearly linear $Hg(CN)_2$ moieties (C−Hg−C = 167−180°), suggesting that this factor governs the magnitude and direction of shielding, with the chloro ligands playing a minor role. In both cases, the shielding is nearly axially symmetric, with the most shielded component

(70) Kim, A. J.; Butler, L. G. *Inorg. Chem.* **1993**, *32*, 178−181.
(71) Duncan, T. M. *Chemical Shift Tensors*; 2nd ed.; The Farragut Press: Madison, WI, 1997.
(72) Gardinier, J. R.; Gabbaï, F. P. *J. Chem. Soc., Dalton Trans.* **2000**, 2861−2865.
(73) Delaigue, X.; Hosseini, M. W.; Kyritsakas, N.; Decian, A.; Fischer, J. *J. Chem. Soc., Chem. Commun.* **1995**, 609−610.
(74) Martin, J. D.; Greenwood, K. B. *Angew. Chem., Int. Ed.* **1997**, *36*, 2072−2075.
(75) Chesnut, D. J.; Haushalter, R. C.; Zubieta, J. *Inorg. Chim. Acta* **1999**, *292*, 41−51.
(76) Corradi, A. B.; Cramarossa, M. R.; Saladini, M. *Inorg. Chim. Acta* **1997**, *257*, 19−26.
(77) Corradi, A. B.; Ferrari, A. M.; Pellacani, G. C. *Inorg. Chim. Acta* **1998**, *272*, 252−260.
(78) Martin, J. D.; Dattelbaum, A. M.; Thornton, T. A.; Sullivan, R. M.; Yang, J. C.; Peachey, M. T. *Chem. Mater.* **1998**, *10*, 2699−2713.
(79) Bowmaker, G. A.; Harris, R. K.; Oh, S. W. *Coord. Chem. Rev.* **1997**, *167*, 49−94.
(80) Bowmaker, G. A.; Harris, R. K.; Apperley, D. C. *Inorg. Chem.* **1999**, *38*, 4956−4962.
(81) Bowmaker, G. A.; Churakov, A. V.; Harris, R. K.; Howard, J. A. K.; Apperley, D. C. *Inorg. Chem.* **1998**, *37*, 1734−1743.
(82) Bowmaker, G. A.; Churakov, A. V.; Harris, R. K.; Oh, S. W. *J. Organomet. Chem.* **1998**, *550*, 89−99.

presumably lying along the NC−Hg−CN (pseudo) axis. Since the symmetry characteristics of the crystal structures do not demand axial symmetry at any of the Hg sites in **6** and **7**, this observation provides further support for the dominating influence of local geometry on the shielding properties. The chemical shielding anisotropies are large, ranging in span from 2300 and 2700 ppm in **7** to over 3000 ppm in **6** (Table 6). These can be compared to 3700 ppm for the linear compounds $Hg(CN)_2$ and $HgCl_2$,[82] 1000 ppm for trigonal planar $[NMe_4][Hg(S^iPr)_3]$,[83] and 0 ppm for tetrahedral $K_2Hg(CN)_4$.[84] Systematic studies[79] have revealed that the shielding anisotropy tends to be largest for linear (two-coordinate) geometries, decreasing with secondary interactions and the concomitant deviations from linearity through to trigonal planar (three-coordinate), and finally decreasing to very small or zero for four-coordinate complexes. Thus, the large shielding anisotropies measured for **6** and **7** reflect the dominance of bent, two-coordinate cyanide geometry.

Whereas the overall extent of shielding anisotropy (Ω) is most sensitive to coordination geometry, the isotropic chemical shift is also related to the number and geometry of ligands about the mercury center. In general, δ_{iso} for two-coordinate Hg is much more shielded (i.e., δ_{iso} more negative) than in three- and four-coordinate compounds. For example, $Hg(CN)_2$ and $HgCl_2$ have $\delta_{iso} = -1396$ and -1625 ppm, respectively,[82] while $[NMe_4][Hg(S^iPr)_3]$ has $\delta_{iso} = -79$ ppm,[83] and δ_{iso} for $K_2Hg(CN)_4$ is -463 ppm.[84] The $\delta_{iso}(^{199}Hg)$ values observed for **6** and **7** are somewhat more deshielded than those known for related linear compounds but are still much more shielded than most three- and four-coordinate mercury compounds, indicating that the electronic environment is indeed dominated by the dicyano character. On the basis of the extremely large range of chemical shielding, and the sensitivity to local bonding effects, ^{199}Hg MAS NMR should be quite useful in studying coordination in mercury complexes. The main impediment is overall signal sensitivity, which proved to be a major problem in the present case; both **6** and **7** had poor signal-to-noise, and it is still unknown why no signal could be observed for **1** and **2**.

The ^{13}C isotropic chemical shifts are remarkably varied, considering the overall structural similarity of the Hg−CN bonds. Typical values of δ_{iso} for cyanide groups range from around 120 ppm for organic nitriles, to 128−139 ppm for square-planar group-10 tetracyanometalates,[70] to 148−162 ppm for tetrahedral cyanometalates, including $K_2Hg(CN)_4$ at $\delta_{iso} = 153.1$ ppm.[69,70,84] Free CN^- in solution appears at 166.2 ppm.[85] The present values span much of this range (Table 6), with **1** ($\delta_{iso} = 144$ ppm) intermediate between the ranges of square-planar and tetrahedral cyanometalates, and **2** ($\delta_{iso} = 166.5$ ppm, 169.0 ppm) even more deshielded than free CN^- (aq). The large difference in δ_{iso} (^{13}C) for the $[Hg(CN)_2Cl]_2$ dimers in **1** and **2** appears at first surprising, given the similarity of the structural units. However, in **1**, the C−Hg−C bond angle (150.7(5)°) is much smaller than in **2** (160.1(6)°), which might be expected to impart significantly different shielding properties due to local orbital orientation and bonding effects. It is also notable that only one peak is measured for **1** with its very similar CN geometries (Hg−C = 2.054(15) and 2.058(16) Å; N−C−Hg = 175.9(13)° and 175.9(14)°; C−N = 1.121(14) and 1.104(15) Å), while two (albeit poorly resolved) peaks appear for the geometrically different cyanides in **2** (Hg−C = 2.056(16) and 2.02(2) Å; N−C−Hg = 177.5(14)° and 175(2)°; C−N = 1.107(14) and 1.126(19) Å). These observations underscore the sensitivity of ^{13}C chemical shifts to subtle geometric effects.

All $\delta_{iso}(^{13}CN)$ values from the extended compounds **6** and **7** appear in the narrow range between 148 and 151 ppm, similar to tetrahedral cyanometalates and to $Hg(CN)_2$ at $\delta_{iso} = 149.5$ ppm.[82] Overlapping peaks and similar bonding geometries obscure more detailed assignments.

J-couplings to ^{199}Hg are clearly visible in the ^{13}C MAS NMR spectra of **6** and **7** (though not in those of **1** and **2**). The values (3250 and 3420 Hz, respectively) are comparable to that measured in $Hg(CN)_2$ of 3158 Hz,[65] and much larger than that of tetrahedral $K_2Hg(CN)_4$, 1540 Hz.[84] Indirect spin−spin couplings in these systems are almost certainly anisotropic, as previously documented for both carbon−mercury and phosphorus−mercury spin pairs;[79] however, no attempt was made to characterize the **J**-tensors in the present case. *J*-coupling to the quadrupolar (spin-$^3/_2$) isotope ^{201}Hg (natural abundance 13.2%) would appear as a distorted quartet with spacings based on $^1J(^{13}C,^{201}Hg) = 1200$ Hz (compound **6**) and 1260 Hz (compound **7**), predicted from the ratio of the magnetogyric ratios ($\gamma_{201}/\gamma_{199} = 0.369$). In fact, they are seldom observed as distinct peaks due to relaxation and broadening from the very large quadrupole moment but may contribute to the baseline hump on which the peaks are situated (Figure 9a).

In summary, the ^{199}Hg shielding tensors and $^1J(^{13}C,^{199}Hg)$ values measured in **6** and **7** reveal that the local electronic environment is dominated by the $Hg(CN)_2$ moiety, with the chloride interactions apparently playing a secondary role in influencing the NMR properties. Isotropic ^{13}C cyano chemical shifts in the isolated dimers **1** and **2** exhibit surprising differences possibly due to variations in the C−Hg−C angles, while $\delta_{iso}(^{13}C)$ values in the extended systems **6** and **7** are clustered closely about those of $K_2Hg(CN)_4$ and $Hg(CN)_2$. Despite inherent difficulties in obtaining high-quality ^{199}Hg MAS NMR spectra in anisotropic systems, the growing body of work in this area indicates that the NMR parameters are sensitive to local structure and bonding, and are potentially very useful in studying mercury coordination polymers.

Acknowledgment. Financial support from NSERC of Canada and Imperial Oil are gratefully acknowledged. The Varian Inova 600 (University of Manitoba) is supported by the Canada Foundation for Innovation and the Province of Manitoba.

Supporting Information Available: Complete crystallographic data in CIF format for all six reported crystal structures. This material is available free of charge via the Internet at http://pubs.acs.org.

IC049792E

(83) Han, M.; Peersen, O. B.; Bryson, J. W.; O'Halloran, T. V.; Smith, S. O. *Inorg. Chem.* **1995**, *34*, 1187−1192.
(84) Wu, G.; Wasylishen, R. E. *J. Phys. Chem.* **1993**, *97*, 7863−7869.
(85) Pesek, J. J.; Mason, W. R. *Inorg. Chem.* **1979**, *18*, 924−928.